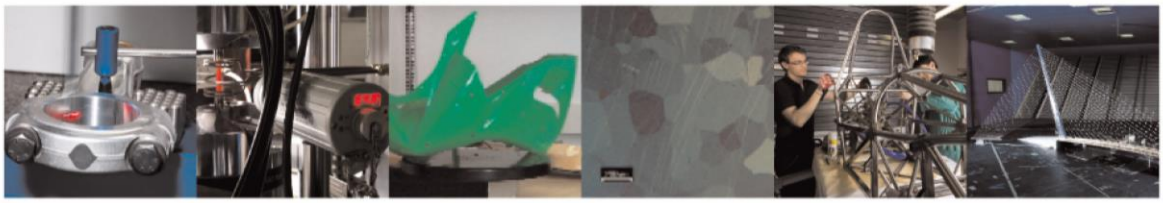

# A model-based approach for online estimation of surface waviness in roll grinding

Parenti, Paolo; Leonesio, Marco; Cassinari, Alberto; Bianchi, GIACOMO DAVIDE; Monno, Michele

This is a post-peer-review, pre-copyedit version of an article published in INTERNATIONAL JOURNAL OF ADVANCED MANUFACTURING TECHNOLOGY. The final authenticated version is available online at: http://dx.doi.org/10.1007/s00170-015-6864-1



DIPARTIMENTO DI MECCANICA ■ POLITECNICO DI MILANO
via G. La Masa, 1 ■ 20156 Milano ■ EMAIL (PEC): pecmecc@cert.polimi.it
http://www.mecc.polimi.it
Rev. 0

# A model-based approach for online estimation of surface waviness in roll grinding

**Paolo Parenti · Marco Leonesio · Alberto Cassinari · Giacomo Bianchi · Michele Monno**

Received: 11 September 2014 / Accepted: 27 January 2015 / Published online: 28 February 2015

## Abbreviations

| | |
|---|---|
| $X_{NOM}$ | Commanded infeed |
| $X_{\mathrm{act}}$ | Actual engaged infeed |
| $X_{\mathrm{disp}}$ | Radial relative displacement due to structural deformation |
| $D_{\mathrm{S,W}}$ | Wheel and workpiece diameter |
| $\omega_{\mathrm{S,W}}$ | Rotational speed |
| $\theta_{\mathrm{S,W}}$ | Angular position |
| $K_{\mathrm{g}}$ | Grinding stiffness |
| $K$ | Specific energy |
| $F_{\mathrm{n}}$ | Normal force |
| $\Delta \mathrm{X}_{\mathrm{S,W}}$ | Radius deviations due to waviness |
| $NL_{\mathrm{S,W}}$ | Number of waviness wavelengths |
| $N_{\mathrm{ov}}$ | Overlaps for average waviness computation |
| $A_{\mathrm{Sj,Wj}}$ | Waviness amplitudes |
| $a_{\mathrm{S_j,W_j}}$ | Complex waviness coefficients |
| $H_{\mathrm{N}}$ | Relative machine dynamic compliance |
| $T$ | Structural dynamic transmissibility |
| $\ddot{\mathrm{X}}_{\mathrm{sens}}$ | Accelerometer readings |
| $X_{\mathrm{KIN}}$ | Instantaneous kinematic wheel infeed |
| $\dot{X}_{\mathrm{act}}$ | Time derivative of actual infeed |
| $X_{\mathrm{ci}}$ | Continuous infeed |
| $b_{\mathrm{cut}}$ | Cutting width |
| $V_{\mathrm{S,W}}$ | Tangential speeds |
| $L\mathrm{c}$ | Contact arc length |
| $K_{\mathrm{gd}}$ | Grinding damping |
| $\varepsilon$ | Correcting exponential coefficient |
| $MRR'$ | Material removal rate per unit cutting width |
| $\Delta\overline{\mathrm{X}}_{\mathrm{S,W}}$ | Mean radius reduction (over one revolution) |
| $NL_{\mathrm{Sj,Wj}}$ | Number of lobes around the perimeter |
| $\mathrm{T}_{\mathrm{obs}}$ | Observation windows length |
| $\varphi_{\mathrm{Sj,Wj}}$ | Phase shifts |
| $\omega$ | Independent variable in fourier domain |
| $H_{\mathrm{cross}}$ | Measured cross FRF between process contact point and measurement points |
| $A$ | Overall closed loop transmissibility |

P. Parenti (✉) · M. Monno
Department of Mechanical Engineering, Politecnico di Milano, via La Masa 1, Milan, Italy
e-mail: paolo.parenti@polimi.it

M. Leonesio · A. Cassinari · G. Bianchi
CNR, Institute of Industrial Technology and Automation, via Bassini 15, Milan, Italy

## 1 Introduction

Grinding is a complex process due to the simultaneous presence of an undefined cutting edge, process nonlinearities, grinding wheel geometry subjected to non-uniform wear,

thermal problems, and many other aspects. Grinding process vibrations frequently represent the main limitation for reaching precise and highly-productive cutting [1]. These can be ascribed to different origins such as unbalances, external excitations, or self-excited vibrations (e.g., modal coupling and regenerative chatter): All of these phenomena produce a similar defect, i.e., a waviness (or chatter marks) on the ground workpiece and/or on the wheel surface [2]. Many different approaches have been proposed over the years for waviness measurement and monitoring, by direct and indirect methods [2]. Direct measurement of the workpiece waviness is normally carried out in post-process by means of different contact or contactless transducers and specific profile and roundness measurement equipment (e.g., Talyrond profilers), while wheel profile measurements are less common especially in industry due to the involved complexity given by the rough and abrasive surface. Most of the times *Fourier Transform*, or other form of signal processing such as *Wavelet Transform*, are exploited [1, 3] to extract significant waviness patterns. Some researchers have developed in-process direct measuring systems (either for grinding wheel or workpiece) for real-time monitoring purposes. For example, in [4], an optical sensor, based on the principle of laser triangulation, is used to measure the topography of the grinding wheel including chatter waviness during a cylindrical external grinding process. In [5], Confocal-White-Light microscopy is exploited for waviness measurement in surface grinding. While direct probing of the grinding wheel surface cannot be done by contact probes, optical methods are applicable. Conversely, their main limitations for in-process uses are related to the protection of the sensor head against coolants and metal swarf and to structural vibration arising from the cutting process. Their cost can represent also a significant issue. On the other side, waviness monitoring can be performed through indirect monitoring methods. Cutting forces and acoustic emission (AE) signals [6–8] are ideal monitoring solutions when a pulsed chip formation occurs with consequent cutting pressure modulation (since the main source of the AE signal is the mechanical stress generated in the wheel-workpiece contact zone). In [9], the roundness profile of the workpiece in cylindrical plunge grinding is correlated with AE signals captured in process. In this work, an empirical threshold, varying on machining configuration, is used thus entailing some possible limitations for the prospective industrial applicability of the solution. Alternatively, acceleration measured on the structure is expected to maximize the monitoring performance in all situations, such as regenerative chatter or forced oscillation caused by an already existing waviness acting in a resonance zone, where large oscillations are produced by vibrational energy accumulation into the system, and not necessary by large pulsating forces [2, 9]. In [10], the impact of process vibration on the achieved surface quality in roll grinders is evaluated through an indirect technique exploiting a position/frequency normalized spectrum. A surface quality index is extracted by weighting, with an empirical exponential function, the acceleration spectra, referred to the axial position along the roll, of all the cycle passes. The main objective of this approach is providing diagnostic warnings to the operator about roll waviness formation but its direct quantification is not provided. Waviness on the wheel side and the distortion caused by structural dynamic are not taken into account. The objective of the present research is the development of a monitoring tool able to quantify indirectly, from acceleration measurements, wheel and workpiece waviness in cylindrical grinding without requiring time consuming and expensive measuring systems. The waviness assessment exploits a model-based approach, describing the machine and process closed loop dynamics.

## 2 Machine and cutting process dynamic modelling

Cutting process instability (e.g., regenerative chatter) is addressed to be one of the main sources of waviness generation in grinding [1]. Nevertheless, the present work is not aimed at describing the growth of vibration during unstable machining: It focus on the steady-state effects where the grown waviness generates a modulation of the actual infeed and then a pulsating cutting force. As claimed in [11, 12], the validity of the assumption relies on the fact that the growth and decay time for grinding vibrations due to grinding wheel wear are large compared to the oscillation period. Under the aforementioned hypothesis, process dynamics effect can be synthesized by the schema of Fig. 1: Wheel/workpiece waviness injects an excitation in the closed loop system constituted by the machine and the grinding process, originating a pulsating force that excites the system; the consequent vibration, that affects the infeed itself, can be revealed by dedicated accelerometers at proper locations on the machine structure. The waviness can be estimated backward, knowing the machine dynamic stiffness, from the oscillations occurring at specific frequencies, depending on wheel and roll rotational velocities.

### 2.1 Waviness model

The proposed method is described referring first to roughing operations in traverse cylindrical grinding, where the axial wheel feed per roll turn is usually equal to the wheel width (i.e., no wheel overlap), with

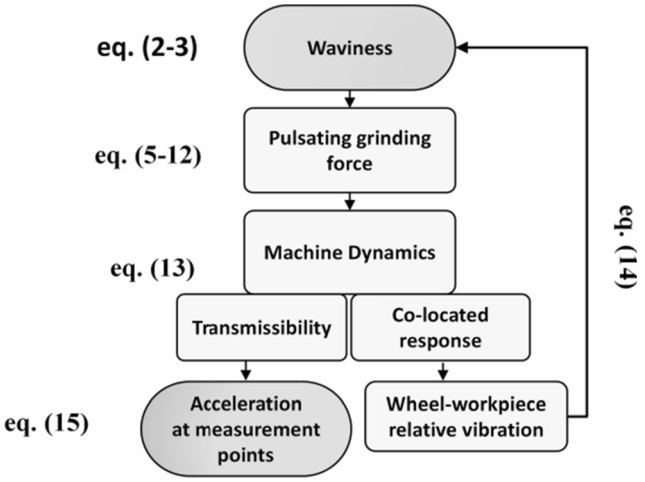


**Fig. 1** Relationship between waviness, machine, and process dynamics and acceleration at measurement points

waviness on both wheel and workpiece. The instantaneous kinematic wheel infeed $X_{KIN}$, in radial direction $X$ (Fig. 2), can be defined:

$$\mathrm{X_{KIN}}(t) = \mathrm{X_{NOM}} + \mathrm{X_{ci}}(\mathrm{t})\text{-}\Delta\overline{\mathrm{X}}_{\mathrm{S}}(t)\text{-}\Delta\overline{\mathrm{X}}_{\mathrm{W}}(t) + [\Delta\mathrm{X_S}(\vartheta_{\mathrm{S}}(t)) + \Delta\mathrm{X_W}(\vartheta_{\mathrm{W}}(t))] \quad (1)$$

where $X_{NOM}$ is the commanded infeed, $\Delta\overline{\mathrm{X}}_{\mathrm{S}}$ and $\Delta\overline{\mathrm{X}}_{\mathrm{W}}$ are the mean radius reduction (over one revolution) due to wear and material removal, $\Delta\mathrm{X_S}$ and $\Delta\mathrm{X_W}$ are the radius deviations due to waviness of wheel and roll, at angular positions $\theta_{\mathrm{S}}$ and $\theta_{\mathrm{W}}$, respectively. Subscripts "S" and "W" refer, in the following, to the grinding wheel and roll, respectively. Usually, an additional time-dependent ramp term $X_{ci}$, called "Continuous infeed", is introduced in order to compensate the radius reduction due to wheel wear represented by the terms $\Delta\overline{\mathrm{X}}_{\mathrm{S}}$ and $\Delta\overline{\mathrm{X}}_{\mathrm{W}}$ in (Eq. 1). In addition, the wheel wear rates are very slow compared to the infeed variation introduced by the waviness, and therefore these three terms in (Eq. 1) can then be neglected. Since in most of the cases, a single chatter frequency arises during an unstable grinding, the waviness shape can be properly assumed as a single sinusoid (Fig. 2). When multiple waviness wavelengths are considered (caused by different chatter frequencies or different rotational speeds), the following general expression holds, respectively:

$$\Delta X_{\mathrm{S}}(\vartheta_{\mathrm{S}}(t)) = \sum_{j=1}^{\mathrm{NL_S}} A_{\mathrm{S_j}}\cdot\sin\left(NL_{\mathrm{S_j}}\cdot\omega_{\mathrm{S}}(t)\cdot t + \varphi_{\mathrm{S_j}}\right)$$
$$\Delta X_{\mathrm{W}}(\vartheta_{\mathrm{W}}(t)) = \sum_{j=1}^{\mathrm{NL_W}} A_{\mathrm{W_j}}\cdot\sin\left(NL_{\mathrm{W_j}}\cdot\omega_{\mathrm{W}}(t)\cdot t + \varphi_{\mathrm{W_j}}\right) \quad (2)$$

where $NL_{\mathrm{S}}$ and $NL_{\mathrm{W}}$ are the number of waviness wavelengths considered, $NL_{\mathrm{Sj}}$ and $NL_{\mathrm{Wj}}$ are the number of lobes around the perimeter for each wavelength, $\omega_{\mathrm{S}}$ and $\omega_{\mathrm{W}}$ are the actual rotational speeds, $A_{\mathrm{Sj}}$, $A_{\mathrm{Wj}}$ and $\varphi_{\mathrm{Sj}}$, $\varphi_{\mathrm{Wj}}$ are the waviness amplitudes and the phase shifts of each single principle.

When finishing operations are addressed, there could be one or more wheel pass overlaps on the same roll surface: In this case, there exist distinct $\Delta\mathrm{X_S}(\theta_{\mathrm{S}})$ and $\Delta\mathrm{X_W}(\theta_{\mathrm{W}})$, one more for each overlap. However, the kinematic infeed can be still computed if the average waviness on $N_{\mathrm{ov}}$ overlaps is considered:

$$\Delta X_{\mathrm{S}}(\vartheta_{\mathrm{S}}(t)) = \frac{1}{N_{\mathrm{ov}}}\sum_{i=0}^{\mathrm{N_{ov}}}\sum_{j=1}^{\mathrm{NL_S}} a_{\mathrm{S_{ji}}}\cdot\sin\left(NL_{\mathrm{S_j}}\cdot\omega_{\mathrm{S}}(t)\cdot t\right) + b_{\mathrm{S_{ji}}}\cdot\cos\left(NL_{\mathrm{S_j}}\cdot\omega_{\mathrm{S}}(t)\cdot t\right)\Delta X_{\mathrm{W}}(\vartheta_{\mathrm{W}}(t))$$
$$= \frac{1}{N_{\mathrm{ov}}}\sum_{i=0}^{\mathrm{N_{ov}}}\sum_{j=1}^{\mathrm{NL_W}} a_{\mathrm{W_{ji}}}\cdot\sin\left(NL_{\mathrm{W_j}}\cdot\omega_{\mathrm{W}}(t)\cdot t\right) + b_{\mathrm{W_{ji}}}\cdot\cos\left(NL_{\mathrm{W_j}}\cdot\omega_{\mathrm{W}}(t)\cdot t\right) \quad (3)$$

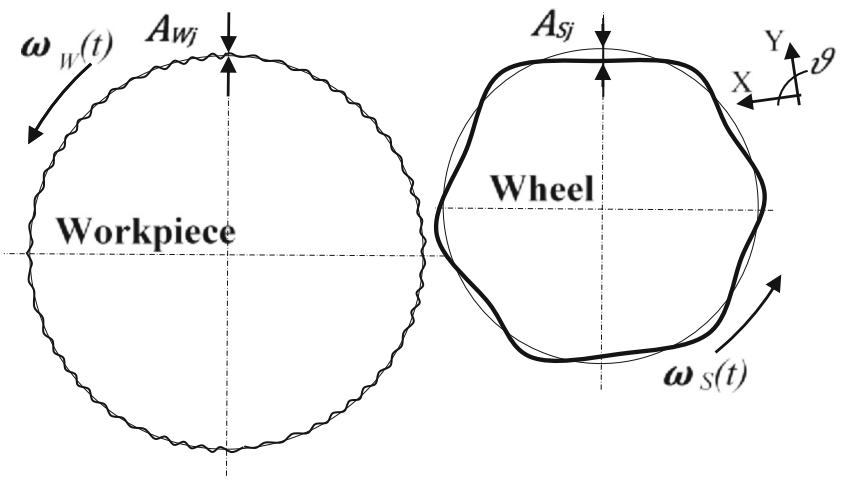


**Fig. 2** Waviness representation on roll and wheel

This latter can be traced back to (Eq. 2), by posing:

$$A_{S_j} = \frac{1}{N_{ov}}\sqrt{\left(\sum_i^{N_{ov}} a_{S_{ji}}\right)^2 + \left(\sum_i^{N_{ov}} b_{S_{ji}}\right)^2}$$

$$\varphi_{S_j} = \tan^{-1}\frac{\sum_i^{N_{ov}} b_{S_{ji}}}{\sum_i^{N_{ov}} a_{S_{ji}}}$$

$$A_{W_j} = \frac{1}{N_{ov}}\sqrt{\left(\sum_i^{N_{ov}} a_{W_{ji}}\right)^2 + \left(\sum_i^{N_{ov}} b_{W_{ji}}\right)^2} \quad (4)$$

$$\varphi_{W_j} = \tan^{-1}\frac{\sum_i^{N_{ov}} b_{W_{ji}}}{\sum_i^{N_{ov}} a_{W_{ji}}}$$

### 2.1.1 Wave filtering

For certain cutting conditions, when vibration amplitude increases, the envelop of the cylindrical wheel shape, registered on the roll surface, is no more an exact sinusoid, due to the *Wave Filtering* effect, where wheel-roll contact occurs along a finite length, introducing a process non-linearity into the system [1, 13]. Moreover, the waviness peak-to-peak may become lower than the double of the wheel-workpiece relative vibration amplitude. On the other side, this phenomenon is not symmetric: When the wheel is asked to run through the roll waviness again, the wheel center peak-to-peak does not undergo attenuation. Therefore, since the distortion effect due to envelop mechanism does not affect the amplitude of the first harmonic of the waviness (see Appendix A), this latter can be exactly traced back to the amplitude of wheel center sinusoidal oscillation.

## 2.2 Grinding force model

The grinding radial force can be assumed to be a function of the material removal rate (MRR), adopting one of the most common expression for the normal force in traverse grinding that considers a quasi-proportionality between the cutting power and the MRR [12]:

$$F_n = K \cdot b_{cut} \cdot \left(\frac{MRR'}{V_S}\right)^{\varepsilon} \quad (5)$$

where $K$ is the specific energy, *MRR'* is the MRR per unit cutting width, $b_{cut}$ is the cutting width, $V_S$ is the tangential wheel velocity, and $\varepsilon$ is a correcting exponential coefficient. In static conditions, when no vibrations occur, the MRR is given by the product of the workpiece speed $V_w$ and the actual engaged infeed $X_{act}$, resulting in a constant force $F_n$. The radial relative displacement $X_{disp}$ caused by structure deformation under the grinding force gives the actual infeed $X_{act}$:

$$X_{act}(t) = X_{KIN}(t) - X_{disp}(t) \quad (6)$$

When vibrations occur, a further dynamic component arises, due to the modulation of $X_{act}$ and, consequently, of *MRR'* [12]: this component can be derived from (Eq. 5) by computing the differential of *MRR'* around its nominal value, in respect to $X_{act}$ and $_{act}$:

$$\Delta F_n = \frac{K \cdot b_{cut}}{V_S^{\varepsilon}} \cdot \left.\frac{\partial (MRR'^{\varepsilon})}{\partial MRR'}\right|_{MRR'_0} \cdot \left(\left.\frac{\partial MRR'}{\partial X_{act}}\right|_{MRR'_0} \cdot \Delta X_{act} + \left.\frac{\partial MRR'}{\partial \dot{X}_{act}}\right|_{MRR'_0} \cdot \Delta \dot{X}_{act}\right) \quad (7)$$

with:

$$MRR'_0 = MRR\left(V_w, X_{act} = \overline{X}_{act}, \dot{X}_{act} = 0\right) \quad (8)$$

then:

$$\Delta F_n = \frac{K \cdot \varepsilon \cdot b_{cut}}{V_S} \cdot \left(\frac{V_W}{V_S} \cdot \overline{X}_{act}\right)^{\varepsilon - 1} \cdot \left(V_w \cdot \Delta X_{act} + Lc \cdot \Delta \dot{X}_{act}\right) \quad (9)$$

It is worth noting that the linearization described by (Eq. 7) represents a good approximation only if the harmonic components of infeed can be considered negligible with respect to its average value so that the contact arc length $L_c$ in (Eq. 9) [13] can be assumed to be constant, over the observation time window:

$$L_C = \sqrt{\overline{X}_{act} \cdot \frac{D_W \cdot D_S}{D_W + D_S}} \quad (10)$$

with $D_W$ and $D_S$ diameters of the workpiece and the grinding wheel, respectively.

Given the stationarity hypothesis, it is useful to switch to the *Fourier* frequency domain, yielding for (Eq. 9):

$$\Delta F_n(\omega) = K_g \cdot X_{act}(\omega) + K_{gd} \cdot \dot{X}_{act}(\omega) \cdot i\omega \quad (11)$$

$$K_g \overset{def}{=} K \cdot \varepsilon \cdot b_{cut} \cdot \left(\frac{V_W}{V_S}\right)^{\varepsilon} \left(\overline{X}_{act}\right)^{\varepsilon - 1}$$
$$K_{gd} \overset{def}{=} \frac{K \cdot \varepsilon \cdot b_{cut}}{V_S} \cdot \left(\frac{V_W}{V_S}\right)^{\varepsilon - 1} \overline{X}_{act}^{\varepsilon - 0.5} \sqrt{\frac{D_W \cdot D_S}{D_W + D_S}} \quad (12)$$

where $\omega$ is the independent variable, $K_g$ and $K_{gd}$ the so-called grinding stiffness and the grinding damping, respectively [12].

2.3 Open loop structural dynamic and system transmissibility

The waviness observer requires an estimate of the radial machine-workpiece relative dynamics, represented via the dynamic compliance $H_N$, in the frequency domain (Fig. 1). $H_N$ can be experimentally identified by adequate measurements. Large machines may have a position-dependent dynamic that should be taken into account in the algorithm by applying appropriate modeling techniques [14]. In this analysis, the system dynamics is assumed constant to limit the complexity of the required model identification in industrial applications: This aspect will be further addressed in future studies. In order to refer the accelerometer readings $\mathrm{X}_{\mathrm{sens}}$ to the process contact area, the structural dynamic transmissibility $T$ is considered:

$$T(\omega) \overset{\mathrm{def}}{=} \frac{H_{\mathrm{cross}}(\omega)}{H_{\mathrm{N}}(\omega)} = \frac{\ddot{\mathrm{X}}_{\mathrm{sens}}(\omega)}{i\omega^2 \cdot \mathrm{X}_{\mathrm{disp}}(\omega)} \tag{13}$$

where $H_{\mathrm{cross}}$ is the measured cross FRF between the process contact point and the sensor's installation point. Different transmissibility functions are computed for each used accelerometer.

2.4 Closed loop frequency response (machine + process)

The relationship between the imposed kinematic infeed $\mathrm{X}_{\mathrm{KIN}}$ and the machine oscillation in the contact area $\mathrm{X}_{\mathrm{disp}}$ can be made explicit by solving the closed loop process dynamics (Fig. 3):

$$\mathrm{H}_{\mathrm{NCL}}(\omega) \overset{\mathrm{def}}{=} \frac{\mathrm{X}_{\mathrm{disp}}(\omega)}{\mathrm{X}_{\mathrm{KIN}}(\omega)} = \frac{\mathrm{H}_{\mathrm{N}}(\omega) \cdot \left(\mathrm{K}_{\mathrm{g}} + \mathrm{K}_{\mathrm{gd}} \cdot i\omega\right)}{1 + \mathrm{H}_{\mathrm{N}}(\omega) \cdot \left(\mathrm{K}_{\mathrm{g}} + \mathrm{K}_{\mathrm{gd}} \cdot i\omega\right)} \tag{14}$$

2.5 Identification scheme of the waviness

By means of proper substitutions involving equations (Eq. 1), (Eq. 2), (Eq. 6), (Eq. 11), (Eq. 13), and (Eq. 14), the basic relation between the measured accelerations to the existing wheel waviness $\Delta \mathrm{X}_{\mathrm{Sj}}$ and workpiece waviness $\Delta \mathrm{X}_{\mathrm{Wj}}$ can be obtained:

$$\ddot{\mathrm{X}}_{\mathrm{sens}}(\omega) = \mathrm{A}(\omega) \cdot \left\{ a_{\mathrm{S_j}} \quad a_{\mathrm{W_j}} \right\} \tag{15}$$

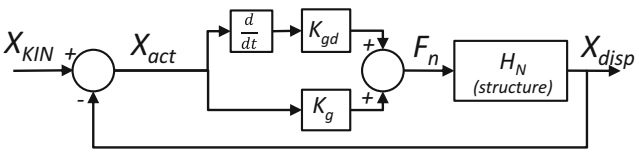


**Fig. 3** Block diagram of the system

where $a_{\mathrm{S_j}}$ and $a_{\mathrm{W_j}}$ are the complex waviness coefficients with amplitudes $A_{\mathrm{Sj}}$, $A_{\mathrm{Wj}}$ and phases $\varphi_{\mathrm{Sj}}$, $\varphi_{\mathrm{Wj}}$, and $A$ is the overall transmissibility between waviness and acceleration at measurement points for the closed loop system. This latter assumes the following expression:

$$\mathrm{A}(\omega) \overset{\mathrm{def}}{=} T(\omega) \cdot i\omega^2 \cdot \mathrm{H}_{\mathrm{NCL}}(\omega) \cdot \left\{ \mathcal{I}\left(\Delta \mathrm{X}_{\mathrm{Sj}}(\theta_S)\right) \quad \mathcal{I}\left(\Delta \mathrm{X}_{\mathrm{Wj}}(\theta_{\mathrm{W}})\right) \right\}^T \tag{16}$$

where $\mathcal{I}$ denotes the Fourier transform. It must be noted that the static and quasi-static contributions of (Eq. 1) are not taken into account in (Eq. 15) and (Eq. 16) that indeed consider only the dynamic related to waviness.

2.6 Batch identification through LS identification

Considering the matrix of (Eq. 15) and (Eq. 16), a *Least Squares* identification method is exploited to identify the waviness in the frequency domain. The identification scheme is compliant with the simultaneous use of different sensors and multiple and overlapped acceleration observation time windows, to improve the identification performance and robustness. The use of *Weighted Least Squares* permits to differentiate the contribution of each sensor to the final estimation, basing on their signal-to-noise ratios and their bandwidths. In the pursued study, since all the sensors are of the same type, they are weighted in the same manner. In order to assure the observability of the waviness coefficients, wheel and workpiece velocities must be chosen accordingly: it is easy to note (Eq. 15) that the excitation frequency of the waviness, on the two sides, must be different. On the contrary, the system becomes ill-conditioned when the two contributes introduce vibrating energy at the same pulsation frequency: In this case, only a total waviness can be estimated, not associated to wheel or workpiece specifically. For instance, in the presence of wheel regenerative chatter, the quantification of the waviness accumulated on the wheel surface requires the two rotational speeds of the wheel/workpiece to be differentiated. The wheel speed can be set to a new value, or a continuous variation law can be adopted. On one side, this allows the algorithm to observe the two waviness contributions but, on the other side, typically introduces some mitigation/suppression effects of the chatter phenomenon [1, 15]: The measurement process disturbs the measured quantity. The waviness identification is then performed in the frequency domain. The main assumption is the steady-state of the vibration response, because system free response is not described in the *Fourier* domain. The typical changing rates of the waviness in grinding [Appendix B] suggest to assume the waviness amplitude as constant during few

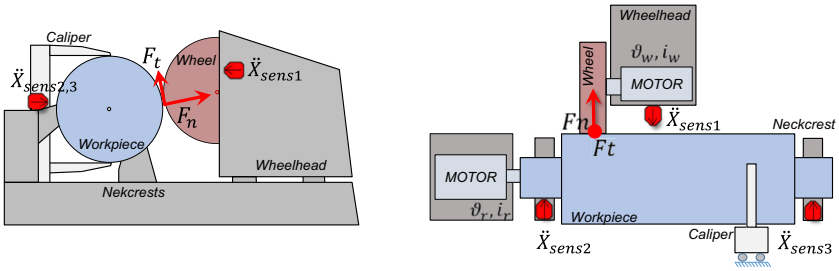


**Fig. 4** Sensors placement on the roll grinder

seconds, which is the usual observation time adopted in the proposed scheme (considering the typical cutting passes duration of 30/40 s in roll grinding). Even the sudden wheel engagements at the begin of the passes, that may generate a sharp rising in the cutting forces, do not pose problem from this point of view because the free response of the machines decays very quickly (as demonstrated experimentally during FRF measurement, on the studied roll grinders, where the lowest significant resonance is around 60/70 Hz with a typical damping of ~3 %. Similar considerations can be done for variable speed operations [1]: The typical variation period adopted for the variation laws (e.g., a sinusoidal spindle speed variation) is of tenths of seconds (according to the available torque at the spindles) thus much greater than the significant vibration periods of the machine.

## 3 Validation of the approach for roll grinding

### 3.1 Experimental set-up

Experimental tests are performed on a roll grinding machine of medium size. A straight profile, mild-steel roll of diameter 507 mm and total length (including roll supports) of 2400 mm, with a uniform hardness of 45±3 HRC, is installed on the machine and supported by two neck rests with friction bearings in white metal. The machine is equipped with a resin bonded wheel (Tyrolit 458AG07H6B1) with a diameter of 790 and 70 mm of width, dressed for roughing cycles (single tip diamond dresser, feed=350 mm/min, depth of cut=5μm). The cutting fluid is a low-foaming synthetic lubricant in 2 % of water mixture, as usually adopted in production stage. The observer scheme is implemented in Labview© on a commercial notebook (Intel i3-2.5 GHz–4 Gb RAM) which is connected to the manufacturer machine supervisor and the Numerical Control (NC Siemens 840d-SL) by using a dedicated Ethernet connection. In this way, several data, coming from the machine numerical control (e.g., velocities, nominal infeed, absorbed cutting power, etc.) are acquired at a sampling rate of 250 Hz. In addition, n°3 piezo-accelerometers (PCB 356A32, 1 V/g) are installed (Fig. 4) on the machine and directly acquired by an A/D board (National Instrument CDAQ + NI9234).

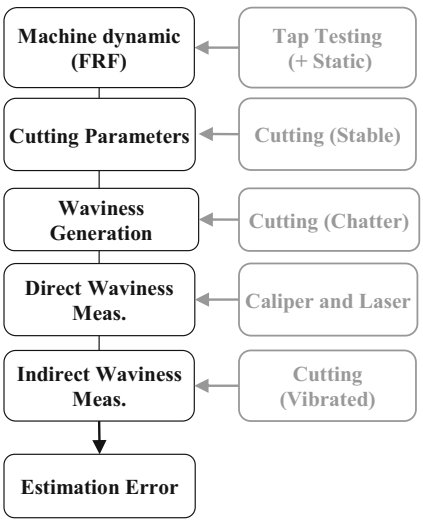


**Fig. 5** Experimental validation procedure

### 3.2 Validation procedure

The assessment of the identification performance on the real system required a validation procedure, shown in Fig. 5 and presented in the following paragraphs.

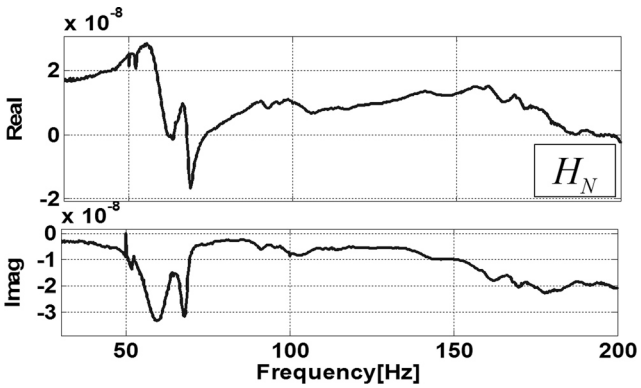


**Fig. 6** Relative dynamic compliance in the radial direction of the machine in the contact zone (Open Loop, i.e., without process)

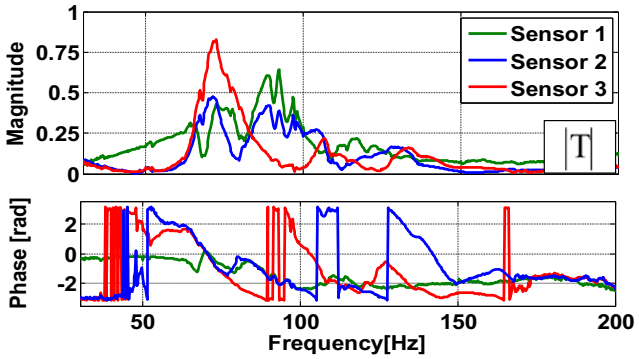


**Fig. 7** Sensor's transmissibility transfer functions (Magnitude and Phase)

### 3.3 Structural dynamic characterization

Tap-testing with instrumented hammer is used to obtain the relative machine FRF in the middle position along the roll (Fig. 6). The system shows two main resonances in the low frequency zone (50–70 Hz), then the dynamic stiffness increases in the middle-high frequency range (80–200 Hz). Due to the method used to excite the structure, FRFs in the low frequency range up to 20 Hz are not reliable. However, no structural resonances are localized in that range. The estimated static machine stiffness in the contact zone is around 64e6 N/m (with a deviation with $Z$-axis positions of ±12e6 N/m). The transmissibility function of each sensor is measured by computing the cross FRF (Fig. 7). It is worth noting that the sensors n°2 and n°3, despite their positioning on the roll neckrests, do not have similar behavior over the frequency range of interest. Above 140 Hz, all sensors decrease significantly their sensitivity in respect to process induced vibration. This is because machine resonances in that zone are involving the spindle shaft, thus generating only localized deflection: In case of high frequency chatter occurrence, the same identification process can be adopted, adding one or more sensors in the spindle region, to assure a better waviness observability. A good transmissibility zone is between 50 and 100 Hz: This suggests the use of this range for the identification: Once the waviness has been generated, it is convenient to move it in that range by properly selecting the wheel and roll speed, compatibly with technological and machine constraints.

### 3.4 Cutting process characterization

To estimate the cutting process coefficients (specific energy $K$ and coefficient $\varepsilon$ in (Eq. 12)), ten cutting grinding passes are performed. To achieve stable cutting conditions, conservative cutting parameters have been adopted and wheel speed has been specifically tuned to avoid chatter conditions in a trial and error way. The model parameters are identified solving a linear regression starting from grinding power measurements and process parameters (spindle power is used as proxy for the tangential cutting force): More details about the identification of these constants can be found in [16]. The identified parameters are $K$=34e9 [J/m$^3$] and $\varepsilon$= 0.91. It must be noted that in all cases where the grinding stiffness is much higher than the machine dynamic stiffness in the frequency range of interest (in this case 0–200 Hz, where more significant machine resonances are located), the following approximation holds:

$$1 + \mathrm{H_N}(\omega)\cdot\left(\mathrm{K_g} + \mathrm{K_{gd}}\cdot i\omega\right) \cong \mathrm{H_N}(\omega)\cdot\left(\mathrm{K_g} + \mathrm{K_{gd}}\cdot i\omega\right) \Rightarrow \quad (17)$$

$$\Rightarrow \mathrm{H_{NCL}}(\omega) \cong 1 \quad (18)$$

In this case process parameters, $K_g$ and $K_{gd}$ estimation has a very limited influence on waviness identification. Consequently, the same can be stated for the actual infeed $X_{act}$. To better evaluate the sensitivity to the identified process stiffness $K_g$ and process damping $K_{gd}$ terms, their values have been artificially increased and decreased (Fig. 8).

It can be noted that the frequency range where $H_{NCL}$ is less sensitive to $K_g$ and $K_{gd}$ is between 100 and 150 Hz: This would suggest the use of this range for identifying the waviness (even if one must strictly consider also the transmissibility functions, Fig. 7). This would preserve the prediction capacity in case of slight changes of the cutting constants in respect to the identified ones. This alleviates the need of performing a fine tuning of the model and makes the identification

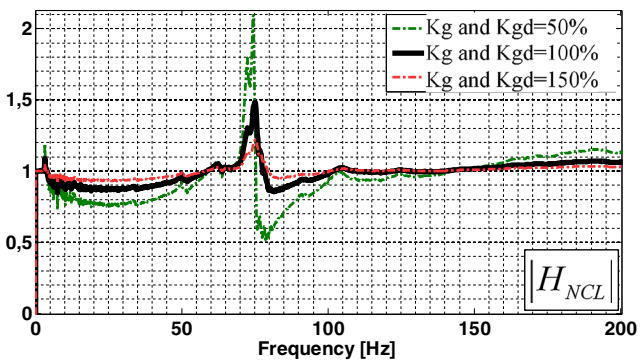


**Fig. 8** Closed loop (machine + process) relative transfer function (magnitude)

**Table 1** Experimental validation: cutting parameters

| Test | Speed during waviness generation [rpm] | | Speed during waviness observation [rpm] | | Traverse speed [mm/min] | | Nominal infeed $X_{NOM}$ [μm] | | Number of lobes | |
|---|---|---|---|---|---|---|---|---|---|---|
| | $\omega_S$ | $\omega_W$ | $\omega_S$ | $\omega_W$ | Generation | Observation | Generation | Observation | $NL_S$ | $NL_W$ |
| #1 | 760 | 30 | 1140 | 37.5 | 2100 | 2625 | 20 | 20 | ~5 | ~126 |
| #2 | 760 | 30 | 1140 | 30 | 2100 | 2100 | 20 | 20 | ~5 | ~126 |
| #3 | 760 | 30 | 1040 | 30 | 2100 | 2100 | 20 | 20 | ~5 | ~126 |
| #4 | 1000 | 30 | 1150 | 26 | 2200 | 1900 | 35 | 35 | ~4 | ~132 |
| #5 | 1000 | 30 | 1150 | 26 | 2000 | 1900 | 35 | 45 | ~4 | ~132 |
| #6 | 1000 | 30 | 1320 | 22 | 2000 | 1615 | 35 | 35 | ~4 | ~132 |
| #7 | 785 | 40 | 1100±10[a] | 34±5[a] | 2933 | 2482±365[a] | 35 | 35 | ~5 | ~98 |
| #8 | 1000 | 25 | 850 | 28 | 1830 | 2050 | 15 | 25 | ~4 | ~160 |
| #9 | 650 | 40 | 728 | 35 | 2930 | 2565 | 15 | 35 | ~6 | ~98 |
| #10 | 1286 | 30 | 1110 | 36 | 2200 | 2638 | 20 | 35 | ~3 | ~128 |

[a] Sinusoidal variation with period of 20 s

approach less sensible to variations that may affect the cutting process such as variation of the lubricant properties. However, particular attention must be paid to the fact that big shifting of wheel and roll speeds, that are necessary to move the waviness in the desired frequency range, must be matched with the technological window of cutting parameters allowed by the system.

### 3.5 Waviness generation

In this phase, the waviness is generated by developing regenerative chatter during cutting. In test #1 (see Tables 1, 2, and 3), the cutting parameters are $V_w$= 30 rpm, nominal infeed=20 μm, traverse feed=2100 mm/min. In the test, the worse wheel speed values are set up in order to get vibration accumulation into the system, according to wheel regenerative chatter theory [12] (no workpiece regenerative chatter is expected since there is no wheel overlap). Figure 9 depicts the vibration growth for wheel speed of 760 rpm. The low growth rate that characterizes wheel chatter regeneration is confirmed (Appendix B) and, after three unstable passes, with a total duration of approximately 90 s, the process is interrupted by abruptly separating the wheel from the roll (the final two passes are shown in Fig. 9). This is done by activating a mechanical safety device that can detach the tool almost instantaneously. The use of this device, that equips the machine for safety reasons, is aimed at preserving the wheel waviness shape and amplitude preventing any modification/reduction during the standard and relatively slow, wheel radial disengagements.

**Table 2** Experimental validation: Fitting errors for the roll waviness

| Test | Root mean square error RMSE [μm] | Normalized root mean square error NRMSE[a] [%] | Normalized root mean square error Cv,RMSE[b] [%] | Mean absolute percentage error MAPE [%] | Maximum absolute error [μm] | Maximum of the percentage error [%] |
|---|---|---|---|---|---|---|
| #1 | 0.66 | 13.17 | 15.19 | 12.47 | 1.88 | 41.01 |
| #2 | 0.84 | 16.78 | 22.40 | 19.88 | 2.73 | 84.03 |
| #3 | 0.766 | 22.37 | 26.60 | 24.84 | 1.39 | 39.87 |
| #4 | 0.72 | 28.21 | 41.77 | 40.51 | 1.45 | 160.65 |
| #5 | 1.78 | 23.52 | 28.81 | 22.72 | 4.88 | 51.68 |
| #6 | 1.26 | 35.85 | 37.27 | 31.78 | 3.04 | 125.10 |
| #7 | 1.372 | 23.38 | 44.57 | 54.68 | 3.29 | 178.65 |
| #8 | 0.37 | 27.37 | 37.01 | 28.68 | 1.10 | 120.95 |
| #9 | 0.82 | 31.11 | 51.71 | 42.98 | 2.20 | 115.06 |
| #10 | 0.45 | 38.99 | 51.82 | 46.28 | 0.95 | 166.53 |

[a] Normalized to the range of the observed data

[b] Normalized to the mean of the observed data

**Table 3** Experimental validation: fitting errors for the wheel waviness

| Test | Error prior to start observation cutting pass [μm,%] | Error after observation cutting pass [μm,%] |
|---|---|---|
| #1 | 1.20 (9.5 %) | 1.03 (12.9 %) |
| #2 | −2.02 (−13.3 %) | 3.10 (31.0 %) |
| #3 | −1.39 (−18.6 %) | −1.21 (−28.6 %) |
| #4 | 0.84 (17.7 %) | 0.10 (11.2 %) |
| #5 | 2.38 (29.8 %) | 0.74 (56.9 %) |
| #6 | 0.05 (2 %) | 0.11 (14.5 %) |
| #7 | −4.34 (−26.5 %) | 1.06 (23.8 %) |
| #8 | −0.86 (−30.6 %) | −0.18 (−7.4 %) |
| #9 | 1.43 (20.4 %) | 0.45 (20.1 %) |
| #10 | 0.6 (17.1 %) | 0.11 (6.4 %) |

The time frequency spectra, in Fig. 9 on the right, shows how in this case vibration is generated by a single frequency chatter.

### 3.6 Direct waviness measurement

Grinding wheel waviness is directly measured for obtaining reference values by means of a laser displacement sensor. A laser triangulation, with resolution and accuracy lower than 0.5 μm [17], is used to measure the wheel profile. Laser source is focalized on the wheel cylindrical surface placed at a distance of 30 mm, and signal is acquired at sampling frequency of 50 KHz. The wheel revolution period is triggered by means of a passive magnetic probe activated by the spindle flange bolts. During the measurement, the wheel is rotating at 750 rpm, with an axial feed of 300 mm/min, so that the laser scansion follows a spiral trajectory with an axial pitch of 0.4 mm per turn (Fig. 10).

The large dimension of the laser spot (around 1 mm), almost two orders of magnitude bigger than the mean diameter of the abrasive particles [13] and two order of magnitude smaller than the waviness length to measure, performs a geometrical filter effect on the "noisy" surface of the grinding wheel, reducing the need for profile filtering in post-process to extract the waviness content. Figure 11 shows the FFT (in amplitude) of the average wheel profile affected by a predominant out-of-roundness error at the fifth lobe, caused by chatter (3-D and Polar plot are lowpass filtered at lobe 100th). The measured peak-to-peak amplitude of the wheel waviness (average value of the 5th lobe, along the wheel width) results in 13.8 μm.

In a specular way, the automated caliper installed on the machine (Fig. 4) is exploited to directly measure the amount of waviness cumulated on the cylinder surface. This contact measuring system, whose main aim is to measure macro-geometry such as straightness and roundness profiles of rolls, has been previously characterized and demonstrated to possess micrometric uncertainty (accuracy less than 0.7 μm), making it suitable to perform also waviness measurements. As expected and as perceived by the visual inspection, at the end of the cutting cycle, the roll surface is affected by a predominant amount of waviness with a wavelength around 12.8 mm (Fig. 12) according to the vibration at around 63 Hz. A spiral measurement with the caliper at axial feed=350 mm/min and $V_w$=5 rpm is performed to estimate the waviness amplitude variation along the roll axial dimension. According to the process vibration level during the last pass (see Fig. 9 at 310–340 s), the cumulated waviness is affected by a significant trend reaching the maximum peak-peak amplitude of 7.8 μm near one end of the roll.

### 3.7 Indirect estimation of the waviness

In this step, cutting tests are executed under the influence of the existing waviness. In this phase, the system acceleration response and the actual speeds of the cylinder and the grinding wheel are recorded. These data, then, feed the identification algorithm creating a stream of "a posteriori" predictions. Chatter frequency and thus waviness orders (i.e., the number of generated lobes) fitted by the identification are set by automatic peak detection on the FFT data. Afterwards, roll and wheel

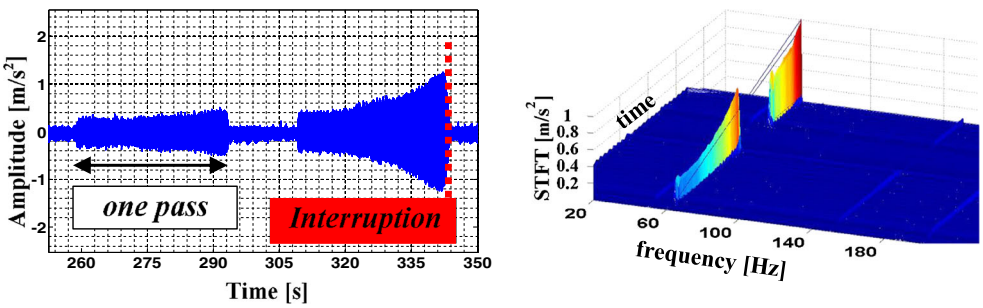


**Fig. 9** Waviness generation phase: raw acceleration in time domain and STFT of Sensor 1

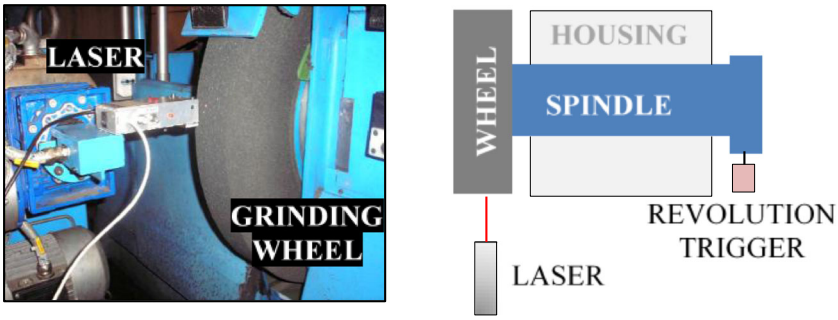


**Fig. 10** Laser sensor setup for wheel waviness direct measurement

speeds are increased by 25 and 50 %, respectively, in order to separate the waviness in two single contributes, making them observable by the algorithm. The choice is performed also considering that a proper wheel speed change improves the cutting stability avoiding generation of new waviness lobes at the new speed value. Lobes diagram theory can support this decision [1]: In this case, optimal tuning is chosen empirically basing on experimentally predetermined values. The waviness contributes on vibration are clearly visible and distinguished in frequency domain as distinct spectral peaks (Fig. 13). As expected, roll waviness is responsible for the smaller peak around 80 Hz while the peak at higher frequency, near 100 Hz, comes from the excitation introduced by the grinding wheel waviness. It can be noted that, in this case, the choice of different observation windows length ($T_{obs}$) does not affect the goodness of the fitting (Fig. 13).

When precise measurements of grinding wheel and cylinder velocities are not available, a coarser spectral resolution (lower $T_{obs}$) is suggested for increasing the robustness of the algorithm. The fitting is performed between 30 and 150 Hz where the dynamic modeling is reliable and the main contributions are expected to fall, considering the machine resonances involved in regenerative chatter. Time overlap of 50 % is used for all the observation windows in order to follow waviness variations with adequate promptness. Data windowing is also applied to avoid leakage in the *Fourier* transform. The estimated and measured waviness on roll and wheel is compared in Fig. 14. Good agreement is found even considering the relevant variation of roll waviness amplitude along the workpiece perimeter and the growing trend along its generating axis that does not agree perfectly with the adopted steady-state assumption for the waviness profile. It is worth noting that the higher fitting error at the beginning of the cutting pass that could be related with the variability of the system dynamics and sensor's transmissibility along the *Z*-axis position. With the use of moving time windows, multiple partially correlated waviness estimations are obtained on overlapped portions of the roll and compared with the same direct measurements performed with the machine caliper before the identification cutting. The maximum absolute fitting error along the profile is of 1.88 μm, the maximum of the percentage error is 41.01 %, the RMSE (root mean square error) is 0.66 μm, the NRMSE (normalized RMSE in respect to the range of the measured quantity) is 13.17 %, and the cvNRMSE (normalized RMSE in respect to the mean of the measured quantity) is 15.19 %. It can be noted that most of the local error is periodic and associated with an oscillation pattern on the estimated waviness. Considering the accuracy of the instruments used for direct waviness measurements, these results are consistent. On the other side, the estimation error

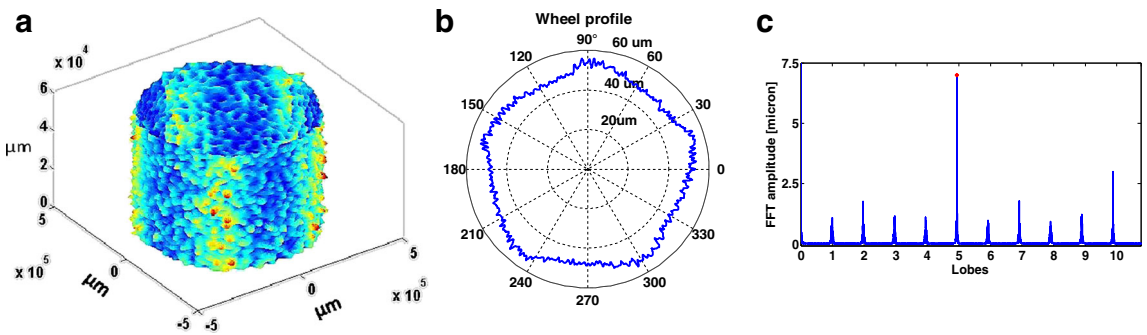


**Fig. 11** Wheel profile measure (laser sensor) after the waviness generation test: **a** 3-D Plot, **b** Polar Plot, **c** FFT plot

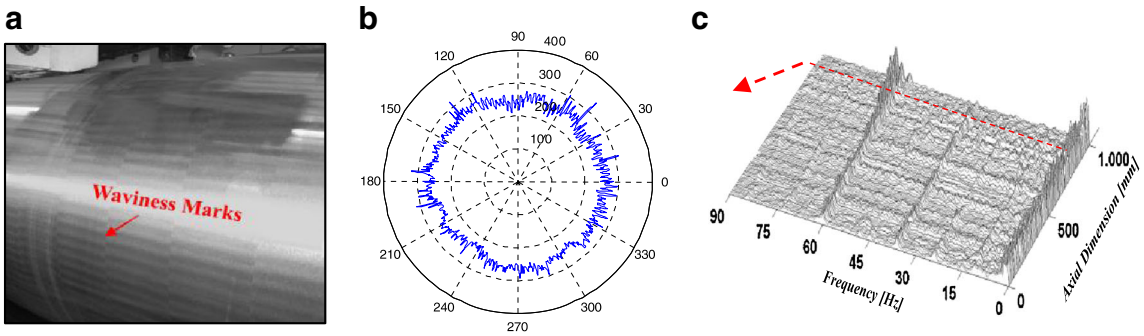


**Fig. 12** Surface Waviness on the roll after the waviness generation test: **a** High contrast B&W picture, **b** caliper polar plot, and **c** Caliper FFT (scaled at the rotational frequency occurred during roll cutting)

on the wheel waviness can only be evaluated at the beginning and at the end of the cutting pass when direct measurements are executed. However, the identification algorithm provides the estimation of wheel waviness decrease rate: In this case, a linear trend is found with a rate of 7 μm/min. The absolute fitting error on the initial wheel waviness results in 1.2 μm (9.5 %) while at the end of the cutting pass it results in 1.03 μm (12.9 %).

Following the same validation procedure, n°10 tests have been conducted (Table 1) under different cutting conditions both for "lobes generation" and "lobes observation" cutting. Different waviness severity has been generated by interrupting the cutting after different vibration amplitudes have been developed into the system. After the observation tests, the wheel has been dressed and stable cutting passes have been performed in order to clean out the residual waviness contributes establishing the original surface conditions on wheel and roll. Despite the high variability of the waviness along the roll profile suggests the use of two different normalized indicators

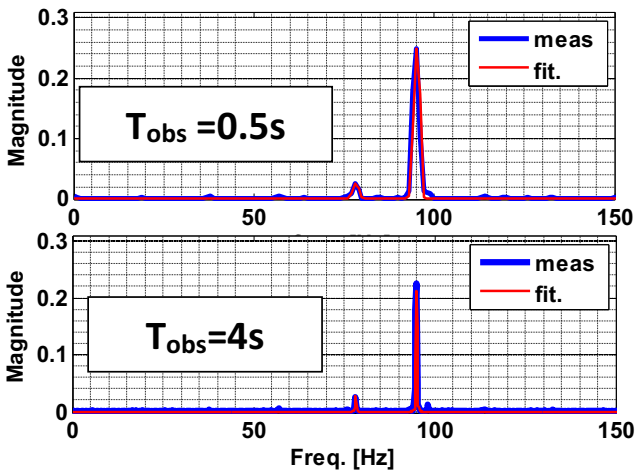


**Fig. 13** Goodness of the acceleration spectrum fitting: fitted magnitude for two different observation length in the middle of the roll position

(*NRMSE* and *cvNRMSE*), they resulted in similar values ranging about from 10 to 50 %, as the *MAPE* indicator.

On the other side, the estimation errors of the wheel waviness are consistent and limited to 30 %. One exception is represented by test #5 where the percentage error is bigger than other tests (i.e., 56.9 %) but the absolute error is still very low and less than 1 μm. The effect of the speed offset applied to observe the two waviness patterns distinctly did not play a key role for the estimation error since all the tests, with different speed offset, provide consistent results. In particular, as can be noticed by test #2 and test #3, good estimation is provided even when the roll waviness is not been moved from the resonance zone meaning that the dynamic modeling can be considered reliable. In test #7 (Table 1), extreme vibrations levels have been reached and the estimation provided by the use of variable speed conditions agrees with the other tests performed at constant rotational speed in terms of *RMSE* but particularly high values of *Maximum Absolute Error* and *Maximum of the percentage Error* have been produced: Further insight will be devoted to this aspect. Considering the variability of the waviness formation process and the complexity and inhomogeneity of the waviness formed on the workpiece, the estimation performance is satisfactory for providing in-process feedback information to grinding operators or to automatic process controllers.

## 4 Conclusion

In this work, an online waviness identification scheme for cylindrical traverse grinding has been developed. Wheel and workpiece waviness generated by process vibration, caused in this case by regenerative chatter, are identified starting from acceleration measurements and exploiting a model-based approach with a *Least Squares* algorithm. The method exploits a model of the waviness, a linearized model of the cutting process

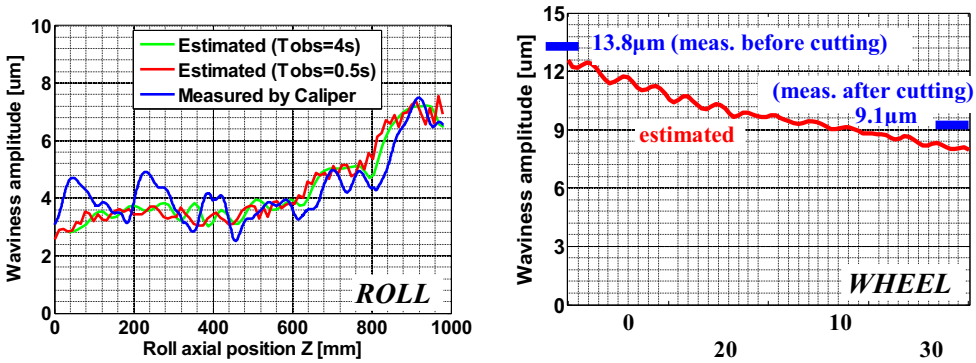


**Fig. 14** Peak-valley amplitude of the waviness on the roll (~126 lobes) and wheel (~5 lobes): direct and indirect measurements

and the machine dynamics (in terms of relative radial compliance between wheel and workpiece and in terms of dynamic transmissibility from the process contact point to sensors location). In this analysis, the machine behavior (i.e., static and dynamic) is considered time-invariant and position independent. These two sets of parameters must be identified prior to applying the algorithm by means of dedicated testing procedures (i.e., cutting test with absorbed cutting power and the actual infeed measurement and dynamic compliance identification by Tap Testing). Experiments on a roll grinding machine confirm that a good online estimation of the waviness can be achieved. This monitoring algorithm can provide a valuable feedback to grinding operators on the actual state of the process and, additionally, support the development of real-time algorithms for automatic grinding process optimization. Further improvements to the implemented waviness monitoring modules can include the adoption of LPV (linear parameter variant) approach for modeling machine dynamic taking into account its variability with the *Z*-axis position.

**Acknowledgments** This work has been supported by funding of the Italian Ministry of Economic Development under the research program *Industria 2015 "Michelangelo"* (D.M. n. 00052MIOl).

## Appendix A: Waviness under wave filtering

Regarding the sinusoid distortion, it can be demonstrated that it does not involve the first harmonic component of the waviness. Namely, the fundamental harmonic component of the disrupted waviness is equal to the amplitude of the sinusoidal vibration that generated it. Thus, if the analysis is restricted to the first harmonic component, process dynamics still remain linear.

Let a sinusoidal profile be considered:

$$\mathbf{P}(x) = \begin{Bmatrix} x \\ \widehat{A}\,\sin(x) \end{Bmatrix} \tag{19}$$

The corresponding circular envelop curve (Fig. 15) is given by the following expression:

$$\mathbf{P}'(x) = env(\mathbf{P}(x)) = \begin{Bmatrix} x \\ \widehat{A}\,\sin(x) \end{Bmatrix} + \frac{R\cdot\mathrm{sign}(\cos(x))}{\sqrt{1+\frac{1}{\cos^2(x)}}} \begin{Bmatrix} 1 \\ \frac{-1}{\cos(x)} \end{Bmatrix} \tag{20}$$

The envelop expression is composed by two addends: The first is the original sinusoid, while the second exhibits a periodicity twice than the first. Given the linearity of *Fourier Transform*, it is straightforward that the first harmonic component coincides with the amplitude of the original sinusoid.

## Appendix B: Waviness growing rate during chatter

The growing rate of grinding chatter can be evaluated by considering Fig. 16 where the relative dynamic compliance between wheel and roll is described in normal directions along with the presence of the delayed feedback loop associated to wheel wear (i.e., that lead the system to wheel regenerative chatter).

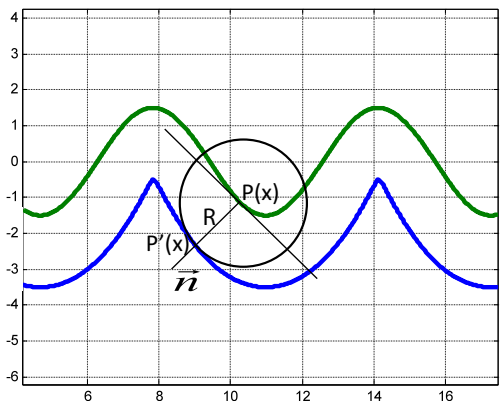


**Fig. 15** Enveloped curve (in *blue*) of a generic sinusoidal profile (in *green*), considering a wheel radius *R*

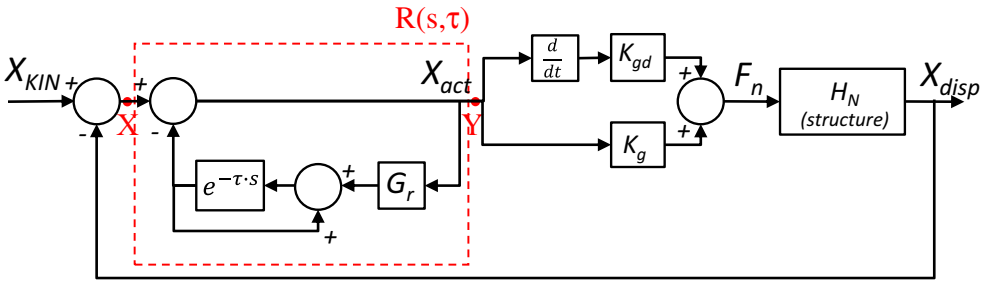


**Fig. 16** Block diagram with wheel regeneration loop

Coherently with (Eq. 21), the radial grinding ratio $G_r$ represents the ratio between the wheel radius reduction and the instantaneous actual infeed; it can be expressed starting from the well-known volumetric grinding ratio $G$ [13] by means of the following expression:

$$G_R = \frac{V_W}{V_S} \cdot G^{-1} \tag{21}$$

The $R(s,\tau)$ is the so-called regeneration loop that represents the amount of wheel wear cumulating at each wheel revolution, that must be subtracted to the actual infeed. It can be made explicit by computing the transfer function between the actual infeed before and after the modulation due to wheel wear ($X$ and $Y$, respectively, in Fig. 16):

$$X - \left( Y \cdot G_r \cdot \frac{e^{-\tau S}}{1 - e^{-\tau S}} \right) = Y \tag{22}$$

and:

$$\mathrm{R}(s,\tau) = \frac{Y}{X} = \left( 1 + G_r \left( \frac{e^{-\tau S}}{1 - e^{-\tau S}} \right) \right)^{-1} \tag{23}$$

The regeneration loop transfer function may be exploited to derive an estimation of wheel wear accumulation rate. Indeed, assuming that a wheel-workpiece relative vibration is imposed (i.e., neglecting the effect of the relative dynamic compliance), $R(s,\tau)$ fully describes the wheel wear evolution.

Let a Padè first-order approximation be applied to $R(\mathrm{s},\tau)$, it yields:

$$R(s,\tau) = \frac{1 - e^{-\tau S}}{1 - e^{-\tau S}(1 - G_r)} \cong \frac{1 - (1 - \tau s)}{1 - (1 - \tau s)(1 - G_r)} = \frac{\tau s}{G_r + \tau (1 - G_r) s} \tag{24}$$

The pole of the system (Eq. 24) can be easily computed, together with its time constant $T_p$ that assumes the following expression:

$$T_p = \tau \cdot \frac{1 - G_r}{G_r} \tag{25}$$

The time constant represents the time in which the system reaches around the 60 % of its final values: Considering a radial grinding ratio $G_r = 0.0032$, (identified in the grinding tests), the (Eq. 25) estimates that the wheel reach around the 60 % of the final wear in about 300τ seconds, that is in 300 wheel revolutions (i.e., 20 s). Coherently with literature [1, 11, 12, 18], these "numbers" suggest that wheel regenerative chatter grows rather slowly compared to workpiece regenerative chatter or other forms of process instabilities.

## References


1. Inasaki I et al (2001) Grinding chatter origin and suppression. CIRP Ann Manuf Technol 50:515–534
2. Tönshoff HK et al (2002) Process monitoring in grinding. CIRP Ann Manuf Technol 51(2):551–571, ISSN 0007-8506
3. Gonzalez-Brambila O et al (2006) Chattering detection in cylindrical grinding processes using the wavelet transform. Int J Mach Tools Manuf 46:1934–1938
4. Brinksmeier E, Werner F (1992) Monitoring of grinding wheel wear. CIRP Ann Manuf Technol 41(1):373–376
5. Biermann D, Feldhoff M (2011) Influence of controlled tool orientation on pattern formation and waviness in surface grinding. Prod Eng 5(1):31–36
6. Gradisek J et al (2003) Automatic chatter detection in grinding. Int J Mach Tools Manuf 43:1397–1403
7. Wakuda M et al (1993) Monitoring of the grinding process with an AE sensor integrated CBN wheel. J Adv Autom Technol 5(4):179–184
8. Varghese B et al (2000) Development of a sensor-integrated "Intelligent" grinding wheel for in-process monitoring. CIRP Ann Manuf Technol 49(1):231–234, ISSN 0007-8506
9. Batako ADL, Goh SY (2014) Workpiece roundness profile in the frequency domain an application in cylindrical plunge grinding. Int J Adv Manuf Technol
10. Wu CY (2003) Surface quality assessment using vibration signals for transverse roll grinding. China Steel Tech Rep 17:37–42

11. Thompson RA (1973) The character of regenerative chatter in cylindrical grinding. J Eng Ind 95(3):858–864
12. Inasaki I, Yonetsu S (1977) Regenerative chatter in grinding. Proc 18th Int Machine Tool Design and Research Conf 423–429
13. Rowe WB (2009) Principles of modern grinding technology. William Andrew, First edition, ISBN: 978-0-81-552018-4
14. Symens W et al (2008) Identification of interpolating affine LPV models for mechatronic systems with one varying parameter. Eur J Control 14(1):16–29. doi:10.3166/ejc.14.16-29
15. Alvarez J et al (2013) Avoiding chatter in traverse cylindrical grinding by continuous workpiece speed variation. J Manuf Sci Eng 135(5):5. doi:10.1115/1.4024820
16. Leonesio M et al (2012) A time-domain surface grinding model for dynamic simulation, 3rd CIRP conference on process machine interactions. CIRP Procedia 4:166–171
17. Norgia M et al (2010) Dedicated optical instruments for ultrasonic welder inspection and control. Measurement 43(1):39–45
18. Marinescu ID et al Handbook of machining with grinding wheels. CRC Press, Taylor & Francis Book, ISBN 9781574446715